

# Anisotropic nonlinear elasticity in a spherical bead pack: influence of the fabric anisotropy

Yacine Khidas\* and Xiaoping Jia†

Université Paris-Est, Laboratoire de Physique des Matériaux Divisés et des Interfaces,  
CNRS UMR 8108, Cité Descartes, 77457 Marne-la-Vallée, France

Stress-strain measurements and ultrasound propagation experiments in glass bead packs have been simultaneously conducted to characterize the stress-induced anisotropy under uniaxial loading. These measurements, realized respectively with finite and incremental deformations of the granular assembly, are analyzed within the framework of the effective medium theory based on the Hertz-Mindlin contact theory. Our work shows that both compressional and shear wave velocities and consequently the incremental elastic moduli agree fairly well with the effective medium model by Johnson *et al.* [J. Appl. Mech. **65**, 380 (1998)], but the anisotropic stress ratio resulting from finite deformation does not at all. As indicated by numerical simulations, the discrepancy may arise from the fact that the model doesn't properly allow the grains to relax from the affine motion approximation. Here we find that the interaction nature at the grain contact could also play a crucial role for the relevant prediction by the model; indeed, such discrepancy can be significantly reduced if the frictional resistance between grains is removed. Another main experimental finding is the influence of the inherent anisotropy of granular packs, realized by different protocols of the sample preparation. Our results reveal that compressional waves are more sensitive to the stress-induced anisotropy, whereas the shear waves are more sensitive to the fabric anisotropy, not being accounted in analytical effective medium models.

PACS numbers: 45.70.-n, 43.35.+d, 81.05.Rm

## I. INTRODUCTION

The study of nonlinear elasticity in granular materials is not only of fundamental interest but also of practical importance in many fields, including soil mechanics and geophysics. Unlike consolidated porous materials such as sedimentary rocks, soils and sintered bead packs, dry granular materials acquire solely its elasticity as a result of the applied stress, forming a very inhomogeneous force network [1, 2, 3, 4, 5, 6]. The mechanical properties of such materials depend strongly on both the contact interactions between grains and the geometric arrangement (i.e. packing structure). The stress dependence of elasticity which originates with these contact forces at the grain level leads to a complex behaviour of the granular medium: nonlinear behaviour, loading-path dependence and stress-induced anisotropy [7]. The change of sound velocity with the applied stress (i.e. acousto-elastic effect) is the characteristic signature of this nonlinear elasticity [1, 4, 8, 9]. The hysteresis often found in the stress-strain experiments of granular media is also associated with the path-dependant nature of the contact forces [6, 10, 11]. Another issue complicating the analysis of the mechanical properties of granular materials arises from the geometric or fabric anisotropy, which is basically related to the mode of grain deposition and the packing structure in a model system like the sphere pack [10, 12]. This fabric anisotropy is important for the mechanical behaviour of granular media such as stress transmission [13], mechanical stability [14] and liquefaction resistance [15].

Photoelastic visualizations [16] and numerical simulations in 2D systems [17, 18, 19, 20] demonstrate that the anisotropy induced by an external load may have two distinct effects: one

leads to an important change of the fabric anisotropy in the contact network, and the other develops an anisotropic force chain network. Understanding the nonlinear elastic responses and the associated stress-induced anisotropy represents a fundamental issue for granular mechanics. The problem may also be important for understanding the jamming phenomena and shear-induced yielding in a more general class of geomaterials formed from granular media [14, 15, 16]. Development of non destructive methods of investigation is therefore desirable for monitoring the evolution of both geometric and mechanical anisotropies in real 3D granular materials, and allows us to gain a more comprehensive insight into their elastic properties along different stress paths.

Sound waves offer a sensitive and non invasive probe of both the structure and the mechanical properties of heterogeneous materials [21, 22, 23, 24]. In a granular medium, sound propagation is controlled to a large extent by the properties of the contact force networks forming the solid frame of the material [4, 8, 25, 26, 27]. The effective medium theory (EMT) has been commonly used to describe both the nonlinear elasticity [1, 6, 12, 28, 29] and sound propagation in the *long-wavelength* limit [1, 4, 30, 31]. These effective medium models are generally based on the Hertz-Mindlin theory at the grain contact and make use of the two main assumptions to obtain a mean field description of the granular elasticity: i) affine approximation or kinematic hypothesis, in which the motion of each grain follows the applied strain, and ii) statistically isotropic distribution of contacts around each grain. However, some acoustic measurements in random packs of glass beads under isotropic loading [4, 32] show that the ratio of bulk modulus  $K$  to shear one  $G$  is significantly larger than the value predicted by the EMT with bonded elastic spheres (no sliding). Numerical simulations reveal that the discrepancies can stem from the failure of the effective medium approximation: the bulk modulus is well described by the EMT but the shear modulus is not, principally because the EMT

\*Electronic address: yacine.khidas@univ-mlv.fr

†Electronic address: jia@univ-mlv.fr

does not correctly allow the grains to relax collectively from the affine motion assumed by the theory [4, 33]. In a recent work, the multiple scattering of *shear* acoustic waves through the stressed glass bead packs shows that sound propagation at *small-amplitude* (or incremental deformation) does not cause any significant rearrangement of the contact force network [26]. This observation leads to a fundamental question as to whether overestimating the shear modulus by the EMT is related with the failure of the effective medium approximation for sound propagation or with the inadequate treatment of micromechanics at the grain contact level [7, 22].

In this paper, we present new results obtained from a granular model system, i.e. a glass bead pack in an oedometric test. We conducted simultaneously the stress-strain measurement and the ultrasound propagation experiment to characterize the stress-induced anisotropy by uniaxial loading. Both measurements of stress fields and elastic moduli via sound velocities parallel and perpendicular to the applied load are analyzed within the framework of the EMT developed by Johnson *et al.* specifically for stress induced anisotropy in the oedometric configuration [29]. The aim of our work is twofold. Firstly, we examine the applicability of the EMT to small- and large-deformation mechanical tests, corresponding respectively to sound propagation and stress-strain measurements. The crucial role of the interaction nature at the grain contact for the appropriate prediction will be discussed. Then, we investigate the respective responses of compressional and shear waves to the elastic anisotropy in granular media. A particular attention is paid to the influence of the fabric anisotropy which is realized by the different sample preparation. Such inherent fabric anisotropy is expected to evolve little under oedometric loading compared to pure shear experiments.

## II. EXPERIMENTS

In order to characterize the anisotropic elasticity of granular materials, we developed an apparatus coupling the mechanical test with the ultrasonic measurement. The schematic diagram of the experimental arrangement is illustrated in Fig. 1. Spherical glass beads of diameter between  $300\ \mu\text{m}$  and  $400\ \mu\text{m}$  are carefully filled in a duralumin cell up to 70 mm in height and closed by the fitted pistons at the top and bottom surfaces. A controlled vertical load is applied to the granular sample across the top piston. The forces re-directed in the horizontal direction are measured by the stiff force sensors placed at the middle of the cell to monitor the stress anisotropy evolution. This special compaction cell is presumed to be rigid enough that the sample experiences a macroscopic uniaxial strain with negligible lateral motion (oedometric test). The solid volume fraction  $\phi$  of the granular assembly is determined by the axial displacement as a function of the applied load. To ensure the measurements of sound velocities in both the vertical ( $z$ -axis) and horizontal ( $x$ -axis) directions, a pair of compressional or shear piezoelectric transducers of diameter 30 mm in contact with the glass beads are placed at the top and bottom pistons, while the other ones are mounted at the lateral walls separated by a distance of 40 mm (see the inset of Fig. 1).

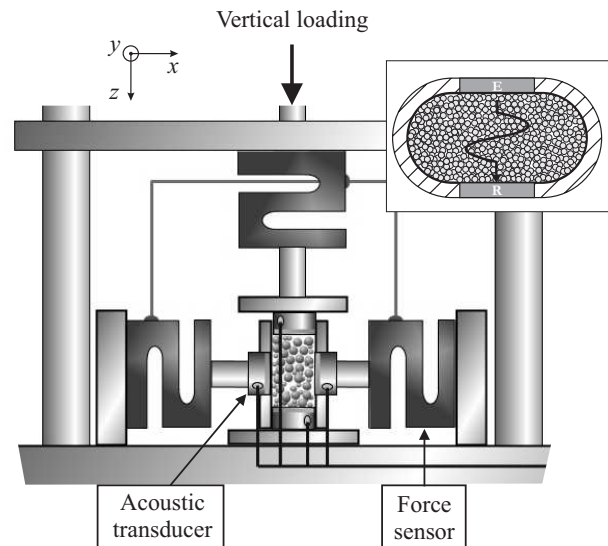


FIG. 1: Sketch of the experimental set-up. Inset: Top-view of the oedometric cell.

### A. Granular fabric and packing density

To study the influence of the granular fabric on the induced elastic anisotropy, the bead packs are realized by two different preparation protocols. The first one, known as rain deposition or air pluviation, consists in pouring the glass beads into the cell through two grids of mesh size 2 mm spaced by 2 cm and reaches a dense pack of  $\phi \approx 0.64$ . The second, termed as de-compaction protocol is to remove gently a horizontal grid through the bead pack from the bottom to the top after filling the beads in the cell; the rearrangements produced by this efficient shearing throughout the sample allow us to obtain a loose pack of  $\phi \approx 0.60$ . It is shown by numerical simulations [17, 34] that the rain deposition protocol creates an anisotropic distribution of the contact angle with two preferred directions orientated roughly at  $30^\circ$  around the vertical (gravity) direction. However, the loose pack prepared by the de-compaction protocol is expected to produce a fairly isotropic distribution of the contact angle [35].

Before any measurement, a preloading up to  $\sigma_{zz} = 400\ \text{kPa}$  is applied to the sample in order to minimize the hysteretic effects related to the grain rearrangements and ensure a reproducible initial state. Then the stress-strain and ultrasonic velocity measurements are performed as a function of the applied stress  $\sigma_{zz}$  ranging from 70 to 900 kPa. Figure 2 displays the evolution of the solid volume fraction  $\phi$  versus  $\sigma_{zz}$  in the dense and loose packs, obtained respectively by the two preparation protocols. These results show a good reproducibility of our sample preparation in terms of the initial packing density measured at  $\sigma_{zz} = 70\ \text{kPa}$  for 30 repeated measurements:  $\phi_{dense} = 0.642 \pm 0.002$  and  $\phi_{loose} = 0.605 \pm 0.002$ . The fact that the solid volume fraction in the dense packing sample is a little larger than the density of the random close packing (RCP) is due to the slight dispersion of the bead size. Furthermore, Fig. 2 shows that the packing density of our sam-

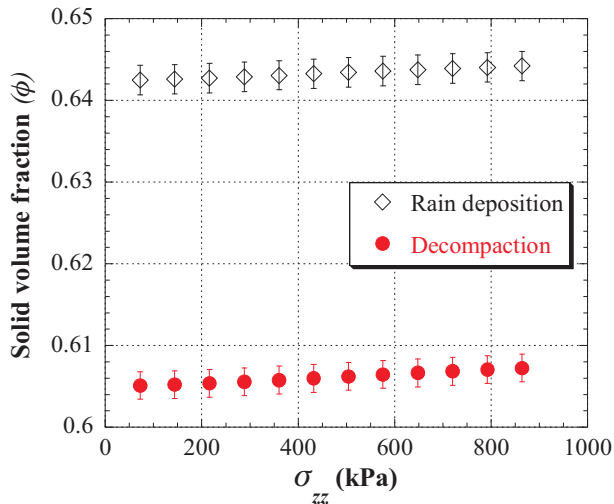


FIG. 2: Evolution of solid volume fraction of the loose and dense packs. Error bars illustrate the data dispersion over 30 measurements.

ples increases slightly, up to a resultant vertical deformation of  $\varepsilon_{zz} (\equiv \varepsilon_3) = 3 \times 10^{-3}$  at the applied  $\sigma_{zz} (\equiv \sigma_3) = 900$  kPa. Both the dense and loose bead packs keep clearly a signature of their preparation protocols. These results imply that for the applied stress in this work, much less than the value to produce the grain fracture of about 20 MPa for the glass beads [36], there are few important rearrangements of grains in the oedometric test as compared to those in a pure shear experiment [16] and the inherent fabric should not change much from the initial state [18].

### B. Anisotropic stress field

Let us now investigate the stress-induced anisotropy under uniaxial loading in the oedometric configuration. By monitoring the resultant horizontal stress  $\sigma_{xx}$  when increasing the vertical stress  $\sigma_{zz}$ , we display in Fig. 3 the stress ratio  $\sigma_{zz}/\sigma_{xx}$  measured as a function of the applied stress  $\sigma_{zz}$  for the two granular samples, respectively. It is observed that both the bead packs evolve from their initial stress fields at low applied  $\sigma_{zz} = 70$  kPa, roughly isotropic, to anisotropic states at high  $\sigma_{zz}$ . As mentioned in the previous experiment [29], the isotropic distribution of stress observed at low  $\sigma_{zz}$  arises probably from a kind of tight wedging of grains produced during the preloading and unloading cycle. Such an interlock of grains may contribute to a residual stress isotropically distributed in the bead pack even when the top piston is removed and no stress is applied.

As the applied stress increases, the ratio  $\sigma_{zz}/\sigma_{xx}$  is seen to increase to an asymptotic value at high  $\sigma_{zz}$ . For the granular packs prepared by the two distinct protocols, the different asymptotic values of about 11% reveal again a memory effect of the initial state of the sample as seen in the above density measurement. In the conventional oedometric test, the inverse of the asymptotic value  $\sigma_{zz}/\sigma_{xx}$  is known as Jacky coefficient  $K_0$  of the earth pressure at rest; it is empirically related to the

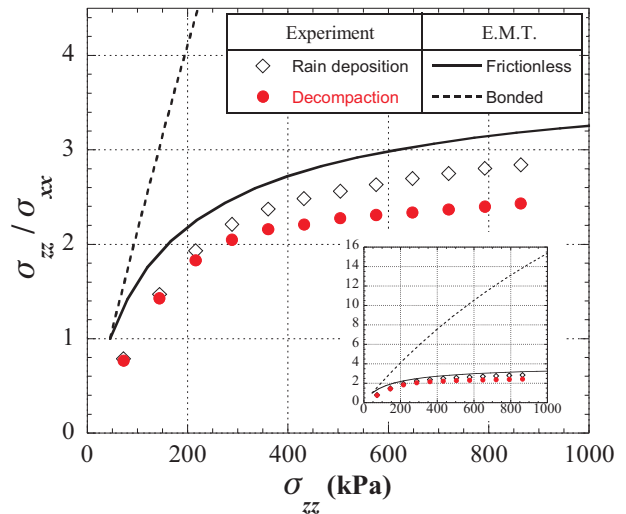


FIG. 3: Evolution of the vertical-to-horizontal stress ratio  $\sigma_{zz}/\sigma_{xx}$  versus the applied stress  $\sigma_{zz}$  in the dense and loose packs.

internal friction angle  $\theta_0$  of the medium by  $K_0 = 1 - \sin \theta_0$  [37]. These results thus suggest a possible correlation between the internal friction angle and the fabric of the medium. To examine this issue, we have measured the avalanche angle  $\theta$  at the relative humidity  $RH = 40\%$  for both the dense and loose packs, and obtained  $\theta_{loose} = 30.4 \pm 1.0^\circ$  and  $\theta_{dense} = 33.2 \pm 0.3^\circ$  for six avalanche experiments. The difference between the two measured avalanche angles is about 9%, consistent with the difference of 11% between the two internal friction angles deduced from the asymptotic values of  $\sigma_{zz}/\sigma_{xx}$  in Fig. 3. Although the avalanche angle is not the direct measure of the internal friction angle, these stress measurements indicates again the significant effect of the preparation protocol on the granular fabric [13, 38].

### C. Anisotropic elastic moduli

Different transports of sound waves in granular media have been detailed in the previous work [39]. When the wavelength is much larger than the bead size, the coherent waves propagate as through an effectively homogeneous medium. Measuring the elastic wave velocity  $V$  allows one to access to the elastic modulus  $M$  of the granular medium by  $M = \rho V^2$  with  $\rho$  the material density [4, 39, 40]. In our apparatus, the compressional P-waves and shear S-waves are excited and detected, respectively, by longitudinal or transversal piezoelectric transducers of diameter 30 mm. Figure 4 displays a typical pulsed ultrasound transmission along the vertical direction. The arrivals of P- and S-wave pulses are well separated, which allows us to clearly identify the different modes and measure adequately the wave velocities by the time-of-flight.

For the granular materials under uniaxial loading and the geometry of the cell considered here, the elastic tensor  $C_{IJ}$  relating the incremental stress  $d\sigma_I$  and strain  $d\varepsilon_J$ ,  $d\sigma_I = C_{IJ}d\varepsilon_J$ , would have a symmetry belonging to the orthotropic class. In such a case, there are nine independent constants as

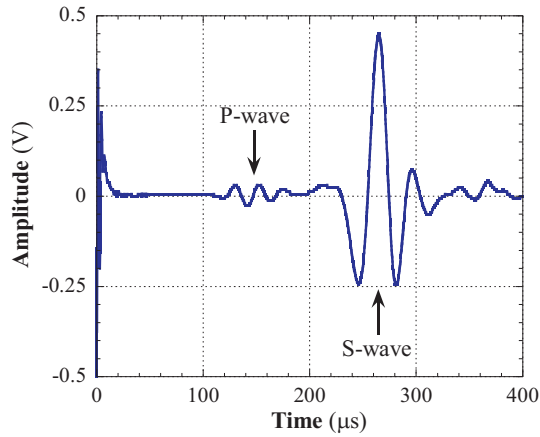


FIG. 4: Typical ultrasound transmission along the vertical direction ( $\sigma_{zz} = 500$  kPa), excited and detected by shear transducers.

shown by the matrix [41]:

$$\begin{pmatrix} d\sigma_1 \\ d\sigma_2 \\ d\sigma_3 \\ d\sigma_4 \\ d\sigma_5 \\ d\sigma_6 \end{pmatrix} = \begin{pmatrix} C_{11} & C_{12} & C_{13} & 0 & 0 & 0 \\ C_{12} & C_{22} & C_{23} & 0 & 0 & 0 \\ C_{13} & C_{23} & C_{33} & 0 & 0 & 0 \\ 0 & 0 & 0 & C_{44} & 0 & 0 \\ 0 & 0 & 0 & 0 & C_{55} & 0 \\ 0 & 0 & 0 & 0 & 0 & C_{66} \end{pmatrix} \begin{pmatrix} d\varepsilon_1 \\ d\varepsilon_2 \\ d\varepsilon_3 \\ d\varepsilon_4 \\ d\varepsilon_5 \\ d\varepsilon_6 \end{pmatrix}.$$

By means of P- and S-waves of different polarization propagating along the horizontal and vertical directions (i.e. principal axes), respectively, we can infer the diagonal elastic components ( $I = J$ ) from the velocity measurement  $C_{II} = \rho V_{II}^2$ . For determining the off-diagonal components, velocity measurements of waves propagating along a direction inclined to the principal axes should be necessary. We display in Fig. 5a and 5b the wave velocities of several elastic waves measured a function of the applied stress  $\sigma_{zz}$  in our loose pack and dense one, respectively. Here  $V_{11}$  and  $V_{33}$  correspond to the velocities of P-waves propagating along the horizontal and the vertical ( $x$ - and  $z$ -axis) directions.  $V_{44}$  denotes to the velocity of the S-wave propagating vertically, whereas  $V_{55}$  and  $V_{66}$  correspond to those of the S-waves propagating horizontally and being polarized along the vertical and perpendicular ( $y$ -axis) directions. Each data presented in Fig. 5 results from an average of six experimental runs and the data dispersion or error-bar is lower than 2% in the case of the loose pack and 3% in the dense sample, illustrating thus a good reproducibility of these acoustic measurements.

As shown in Fig. 5a for the loose pack, there is a clear difference of P-wave velocity between  $V_{11}$  and  $V_{33}$  ( $> V_{11}$ ) going up to 15% when the stress  $\sigma_{zz}$  is increased to 900 kPa. For the S-wave, the velocity difference  $V_{44} > V_{55} > V_{66}$  is less important than that of P-wave: indeed, at  $\sigma_{zz} = 900$  kPa  $V_{44}$  is about 5% and 8% greater than  $V_{55}$  and  $V_{66}$ , respectively. In contrast to the previous works under load superior to a few MPa [4, 29, 32], our acoustic measurements are realized at much lower stress, ranging from 70 kPa to 900 kPa. In such range of loading, it is expected that both the solid volume fraction  $\phi$  (Fig. 2) and the coordination number  $Z$  would vary little

[4]. As the de-compaction protocol tends to create an isotropic fabric in the loose granular sample, our measurements indicate that the elastic anisotropy observed here shall stem from the induced stress anisotropy shown in Fig. 3.

For the dense pack prepared by rain deposition, Fig. 5b displays again a significant difference between the P-wave velocities  $V_{11}$  and  $V_{33}$ . When the anisotropy of the stress field is developed, such elastic anisotropy rises to 18% at  $\sigma_{zz} = 900$  kPa. Unlike the P-wave velocity, the S-wave velocity appears to be sensitive to the fabric anisotropy produced by rain deposition in the dense granular pack. Contrary to the measurement in the loose packing, we observe a significant difference between  $V_{44} = 306 \pm 2$  m/s,  $V_{55} = 342 \pm 7$  m/s and  $V_{66} = 333 \pm 6$  m/s at the lowest stress  $\sigma_{zz} = 72$  kPa where the stress field is nearly isotropic (see Fig. 3). Moreover, when  $\sigma_{zz}$  is increased the S-wave velocities evolve differently, but recover a similar behaviour at high load: a difference of 8% is found again between  $V_{44}$  and  $V_{66}$  at  $\sigma_{zz} = 900$  kPa. These results imply a particular sensitivity of S-wave to the fabric anisotropy which affects the elastic anisotropy together with the stress anisotropy.

### III. COMPARISON WITH THE EFFECTIVE MEDIUM THEORY

The theory of elasticity a granular pack is primarily based on the Hertz-Mindlin model of contact between grains [42]. The macroscopic stress-strain relations are commonly derived using the effective medium description, where it is assumed that the motion of grains is affine with the applied macroscopic strain at least on average, and the distribution of contacts is statistically isotropic and homogeneous. Because the presence of the tangential forces at the contacts gives rise to load-displacement relations which are not only nonlinear but also inelastic, the mechanical response of the medium, namely stress-strain relations, must be expected to depend on the entire past history of loading. However, it is shown that the incremental response of the medium, i.e. the second-order effective elastic constants and consequently sound velocities are path-independent of loading [7]. Within the framework of the effective medium approach, Walton [28] analyzed the mechanical responses of a random pack of identical elastic spheres under isotropic strain and purely uniaxial compression, respectively. Furthermore the incremental elastic moduli were derived for these specific initial deformed states. For simplicity the spheres were assumed to be either *infinitely rough* or *perfectly smooth* in the calculations; nevertheless these results provide a physical insight of the effect of friction in real grain contacts.

As noted above, our measurements were made in the compaction cell with rigid walls in which the granular sample is subjected neither to purely isotropic nor uniaxial compression. To compare with the experimental data obtained in such widely used oedometric tests, Johnson *et al.* proposed an analytical model based on the effective medium theory [29]. This model combines isotropic and uniaxial strains to describe the stress-induced elastic anisotropy in transversely isotropic

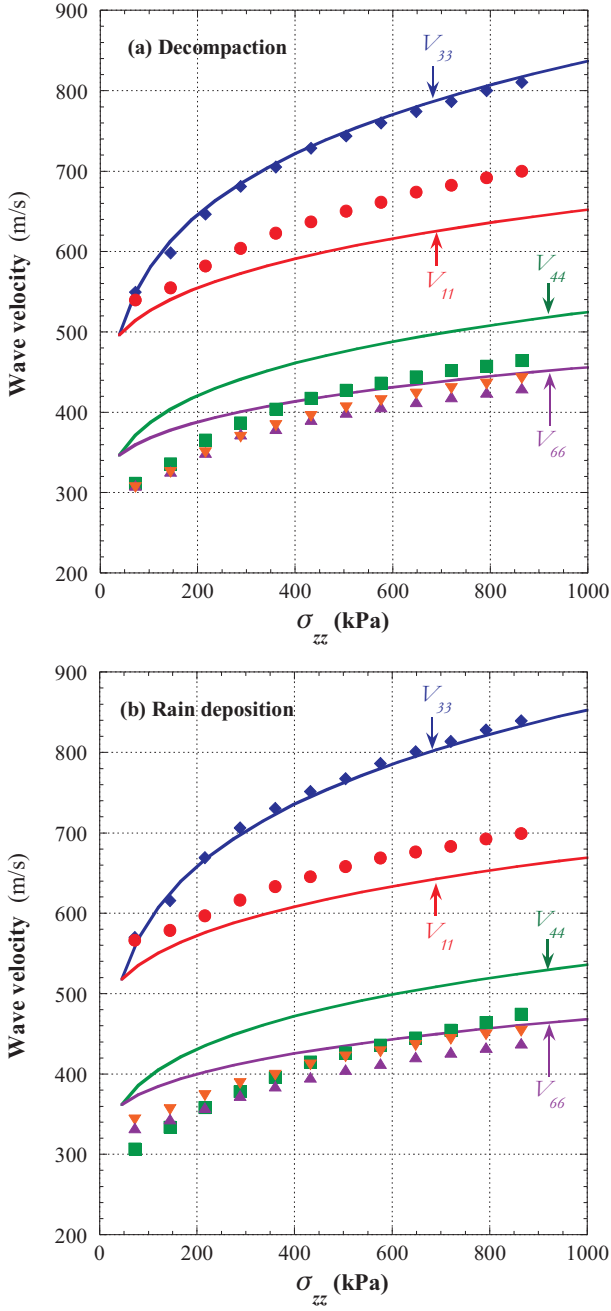


FIG. 5: Wave velocity versus applied stress  $\sigma_{zz}$  in the loose pack (a) and the dense one (b). Experimental data ( $\blacklozenge$ :  $V_{33}$ ,  $\bullet$ :  $V_{11}$ ,  $\blacksquare$ :  $V_{44}$ ,  $\blacktriangledown$ :  $V_{55}$  and  $\blacktriangle$ :  $V_{66}$ ) are compared to the EMT predictions (lines).

granular materials:  $\varepsilon_{ij} = \varepsilon\delta_{ij} + \varepsilon_3\delta_{i3}\delta_{j3}$  with  $\delta_{ij} = 1$  if  $i = j$ , otherwise  $\delta_{ij} = 0$ . Here the internal strain  $\varepsilon$  stems from the residual stress distribution, namely an initial isotropic stress state produced by the preloading-unloading process as mentioned above, whereas the axial strain  $\varepsilon_3$  results from the applied stress  $\sigma_{zz}$ . As  $V_{55}$  differs from  $V_{44}$  only by 5% (Fig. 5), the approximation of the transverse isotropy used in this model would be adequate for interpreting our measurements. The predictions of such a model reduce to the results for purely isotropic compression in the limit  $\varepsilon_3 \rightarrow 0$  and to those

for purely uniaxial compression in the opposite limit  $\varepsilon \rightarrow 0$ , respectively [28].

Fig. 3 presents the ratio  $\sigma_{zz}/\sigma_{xx}$  computed for the packs of both bonded ("rough") and frictionless ("smooth") spheres, as a function of the applied stress  $\sigma_{zz}$ . The latter case is obtained by canceling the tangential contact stiffness in the model, i.e.  $C_t \rightarrow 0$ . As described in eqs. 21 and 22 of [29], the stress tensor  $\sigma_{ij}$  is a function of several parameters,  $\sigma_{ij} = \sigma_{ij}(\varepsilon, \varepsilon_3, Z, \phi, \mu_g, \nu_g)$  where  $Z$  is the coordination number,  $\mu_g$  ( $= 24\text{MPa}$ ) is the shear modulus and  $\nu_g$  ( $= 0.2$ ) is the Poisson ratio of the glass bead. For a given  $C_t$  the ratio  $\sigma_{zz}/\sigma_{xx}$  versus the applied stress  $\sigma_{zz}$  is only parameterized by the glass bead property  $\mu_g$  and  $\nu_g$  (Fig. 3). The axial strain  $\varepsilon_3$  is measured from the displacement of the top piston versus  $\sigma_{zz}$  and the residual isotropic strain  $\varepsilon$  is deduced from the isotropic residual stress 70 kPa measured at  $\varepsilon_3 = 0$ , yielding  $\varepsilon = 1.5 \times 10^{-4}$ .

We observe from Fig. 3, that the theoretical curve calculated with the frictionless spheres ( $C_t \rightarrow 0$ ) is faithful to the qualitative trend observed in our experiments and is overall in agreement with the measured data; at the high load the stress ratio approaches to the limit value of uniaxial loading, i.e.  $\sigma_{zz}/\sigma_{xx} = 4$  [28, 29]. In contrast, Fig. 3 and the inset show that the no-slip assumption with bonded spheres gives rise to a huge overestimation of this stress ratio, indicating the crucial role of the contact interaction law in the effective medium model for describing adequately the evolution of the stress field anisotropy. We may understand the discrepancy found with the bonded spheres by the following picture. At large deformation applied here of the order of  $10^{-3}$ , the grains need to rearrange in order to relax the tangential stress accumulated at the contacts. The no-slip assumption with infinitely frictional spheres forbidden such a process and hence fail, whereas the effective medium analysis with frictionless spheres allow the stress relaxation and provide thus an adequate description of the experiments.

Let us now examine the applicability of the effective medium approach to the wave velocity measurements. Given a stress state  $\sigma$  and corresponding macroscopic deformation  $\varepsilon$ , the elastic moduli can be derived from the incremental stress of the medium subject to an incremental strain by  $d\sigma_{ij} = C_{ijkl}d\varepsilon_{kl}$ . Following the work of [29], yields

$$C_{ijkl} = \frac{3\phi Z}{4\pi^2 R^{1/2} B(2B + C)} \langle \xi^{1/2} \{ 2C n_i n_j n_k n_l + B(\delta_{ik} n_j n_l + \delta_{il} n_j n_k + \delta_{jl} n_i n_k + \delta_{jk} n_i n_l) \} \rangle \quad (1)$$

where  $B = \frac{1-\nu_s}{2\pi\mu_s}$ ,  $C = \frac{\nu_s}{2\pi\mu_s}$ ,  $\xi = -\mathbf{n} \cdot \boldsymbol{\varepsilon} \cdot \mathbf{n}R$ , and  $\delta_{ij}$  denotes the Kronecker symbol. The brackets  $\langle \rangle$  represent an average over all unit vector  $\mathbf{n}$  uniformly distributed since the distribution of contact angle (i.e. granular fabric) is assumed to be isotropic. To determine the wave velocities from the elastic moduli in eq. 1, we perform the calculations by two steps. Firstly, we compute the stress state of a frictionless spheres packing ( $C_t = 0$ ) created by the large axial deformation, which provides an adequate description of the experimental stress field shown in Fig. 3. Then, we consider the appropriate value of  $C_t$  ( $\neq 0$ ) according the Hert-Mindlin theory to calculate the elas-

tic moduli by eq. 1. Note that this procedure of computation is also used in many numerical simulations where the friction between the particles is turned off during the packing preparation and is turned on to measure the incremental response [4]. Fig. 5a and 5b illustrate the calculated wave velocities in both the loose packing and the dense one. The agreement between the theoretical predictions and experimental results remains fairly good (better than 10%), for the present effective medium model employing only one adjustable parameter, i.e.  $Z = 6$  in the dense pack and  $Z = 5.5$  in the loose pack.

## IV. DISCUSSIONS

### A. Stress dependence of P-wave velocities

Based on the Hertz-Mindlin theory of contact and the assumption of isotropic fabric in the sphere pack, the effective medium theory (EMT) predicts a power-law dependence of the elastic modulus  $M \sim P^{1/3}$  (or  $V \sim P^{1/6}$ ) on isotropic compression  $P$  [1, 4, 30, 31]. The same power law scaling is found for the pure uniaxial loading (i.e.  $\varepsilon_{ij} = \varepsilon_3 \delta_{i3} \delta_{j3}$ ) as  $M \sim \sigma_{zz}^{1/3}$  or  $M \sim \sigma_{xx}^{1/3}$  since the stress ratio  $\sigma_{zz}/\sigma_{xx}$  is constant [28]. Numerous acoustic velocity measurements in sands and glass bead packs showed however that the exponent in the power-law scaling may not be constant, varying from 1/4 at low pressure to 1/6 at high pressure [1, 8, 43, 44]. Several mechanisms have been proposed to explain this discrepancy, including the contact recruitment by buckling of particle chains or the conical contact due to irregular surfaces [1], the effect of soft shell on coated spheres [45] and the fluctuation of the stress field [46]. However, for the *preloaded* glass bead packs and the range of the applied stress considered here, the contact recruitment is expected to have a negligible effect, as that suggested by the above density measurement (Fig. 2).

We investigate here the influence of the stress anisotropy on the scaling behaviour of the P-wave velocity. To do this, we displays in Fig. 6 the rescaled P-wave velocities  $V_{33}/\sigma_{zz}^{1/6}$  and  $V_{11}/\sigma_{zz}^{1/6}$  as a function of the applied axial stress  $\sigma_{zz}$ , obtained in the loose and dense packs, respectively. For  $\sigma_{zz} > 300$  kPa,  $V_{33}$  is seen to follows adequately the scaling of  $\sigma_{zz}^{1/6}$ , as expected within the framework of the Hertz-Mindlin theory. By contrast,  $V_{11}$  deviates drastically from the  $\sigma_{zz}^{1/6}$  scaling, which is due to the evolution of stress-field anisotropy illustrated in Fig. 3. Indeed, if rescaling  $V_{11}$  with the stress  $\sigma_{xx}$  parallel to the propagation direction, we recover a scaling behaviour  $V_{11} \sim \sigma_{xx}^{1/6}$  (insets to Figs. 6a and 6b), similar to those for  $V_{33} \sim \sigma_{zz}^{1/6}$  in both the loose and the dense packs having the different granular fabric.

### B. Stress and fabric dependences of S-wave velocities

Compared to the P-wave velocity, the stress dependence of the S-wave velocity is more complicated and strongly influenced by the fabric of the pack. As mentioned above (in sec. II), S-waves are not only sensitive to the stress field anisotropy

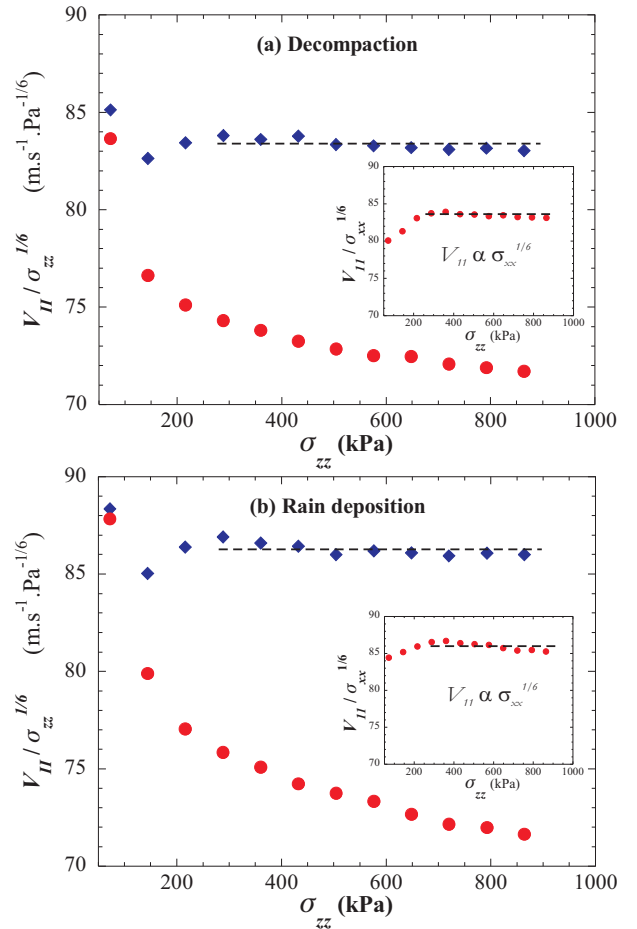


FIG. 6: Stress dependence of P-wave velocities propagating vertically ( $\blacklozenge$ :  $V_{33}$ ) and horizontally ( $\bullet$ :  $V_{11}$ ) in the loose pack (a) and the dense one (b). The dashed lines correspond to the predictions by Hertz-Mindlin theory of contact.

but also to the fabric anisotropy. Let us first examine the scaling behaviour of the shear velocities versus  $\sigma_{zz}$  in the loose bead pack with isotropic fabric. As shown in Fig. 7a, both  $V_{44}$  and  $V_{55}$  scale roughly as a power law i.e.  $\sim \sigma_{zz}^{1/6}$  for  $\sigma_{zz} > 300$  kPa, which agree fairly well with the stress-dependence predicted by the Hertz-Mindlin theory of contact. Compared to the P-wave velocity  $V_{11}$ , the scaling behaviours of the shear velocity  $V_{55}$  is somewhat surprising, however, it may be understood by a heuristic picture which accounts for both the propagation direction and the polarization. Indeed, unlike the P-wave propagating in the horizontal direction ( $V_{11}$ ), the S-wave travelling along the  $x$ -axis is polarized vertically along the  $z$ -axis ( $V_{55}$ ) and it would also be affected by the stress component  $\sigma_{zz}$ . This scenario is consistent with the preceding observation showing that the S-wave velocity is less sensitive to the stress-field anisotropy than the P-wave velocity is (shown in Fig. 5). However, for the S-wave travelling along the  $x$ -axis but polarized horizontally along the  $y$ -axis ( $V_{66}$ ), Fig. 7a shows a scaling behaviour of  $V_{66}$  deviated from  $\sigma_{zz}^{1/6}$  but being consistent with the power law  $V_{66} \sim \sigma_{xx}^{1/6}$  (inset to Fig. 7a), a situation reminiscent to that of the P-wave ( $V_{11}$ ).

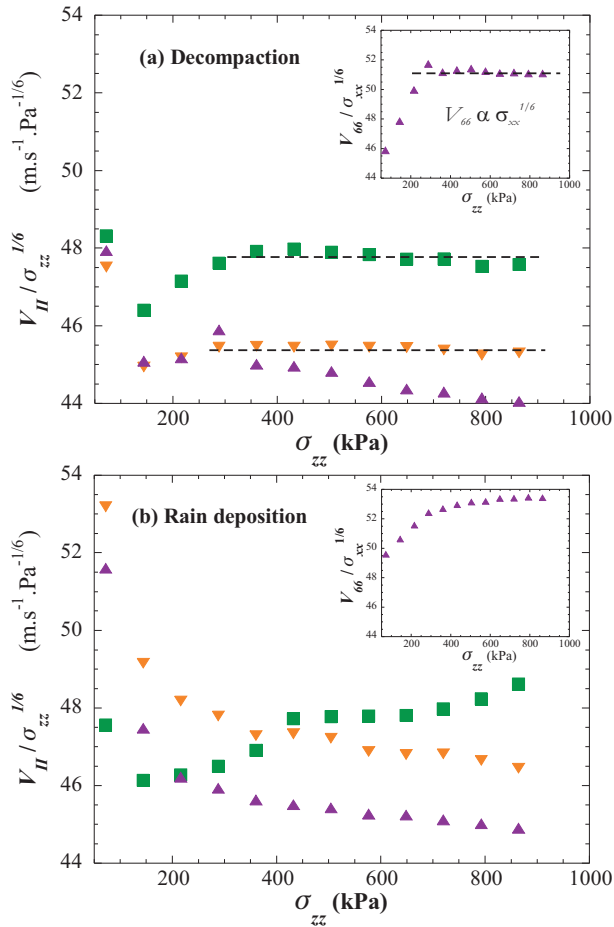


FIG. 7: Stress dependence of S-wave velocities propagating vertically ( $\blacksquare$ :  $V_{44}$ ) and horizontally ( $\blacktriangledown$ :  $V_{55}$  and  $\blacktriangle$ :  $V_{66}$ ) in the loose pack (a) and the dense one (b). The dashed lines correspond to the predictions by the Hertz-Mindlin contact theory.

We now turn on the scaling behaviour of the S-wave velocities in the dense pack presenting the fabric anisotropy obtained by rain deposition. Contrary to the behaviours observed in the loose packing with isotropic fabric, there is no clear stress dependence of the shear velocities  $V_{44}$ ,  $V_{55}$ , and  $V_{66}$  in the range of the applied stress (Fig. 7b and the inset). This observation reveals the extreme sensitivity of the shear wave velocity to the fabric of the granular pack. However, at the present stage, it is difficult to speculate the scaling behaviour of the S-wave velocity on stress, due to the interplay between the evolution of the stress anisotropy and the inherent fabric anisotropy. Indeed, the latter parameter is not included in most of analytical models within the framework of the effective medium theory.

### C. Correlation between induced elastic anisotropy and stress-field anisotropy

In the above sections, we have observed that the elastic moduli and consequently sound velocities (P- and S-waves)

depend on both the induced stress-field anisotropy and the inherent fabric of the granular sample. The protocols of the sample preparation used here, i.e. de-compaction and rain deposition, allow us to obtain two distinct granular fabrics which also differ in the packing density  $\phi$  as shown in Fig. 2 and probably in the coordination number  $Z$ . As suggested by eq. (1), we may investigate the correlation between the induced stress anisotropy and the elastic anisotropy via the ratio of elastic components dropping thus the parameters  $\phi$  and  $Z$ .

Fig. 8a displays the ratio of the compressional moduli  $C_{33}/C_{11}$  versus the induced stress anisotropy  $\sigma_{zz}/\sigma_{xx}$  for two granular samples with different fabric (loose and dense). The experimental data agree well with the effective medium model (eq. 1), demonstrating that the anisotropy of compressional moduli is principally determined by the stress field anisotropy and is much less sensitive to the fabric of the granular pack. Also, we depict the evolution of the shear modulus ratio  $C_{44}/C_{66}$  as a function of  $\sigma_{zz}/\sigma_{xx}$  in Fig. 8b. These results confirm again the correlation of the elastic anisotropy with the stress-field anisotropy, though the anisotropy is less pronounced for the shear modulus than for the compressional one. In contrast to the latter, the shear moduli are however very sensitive to the granular fabric. For the loose pack with isotropic fabric, the ratio of the shear moduli is in good agreement with the effective medium theory model based on the assumption of the isotropic distribution of contact angle.

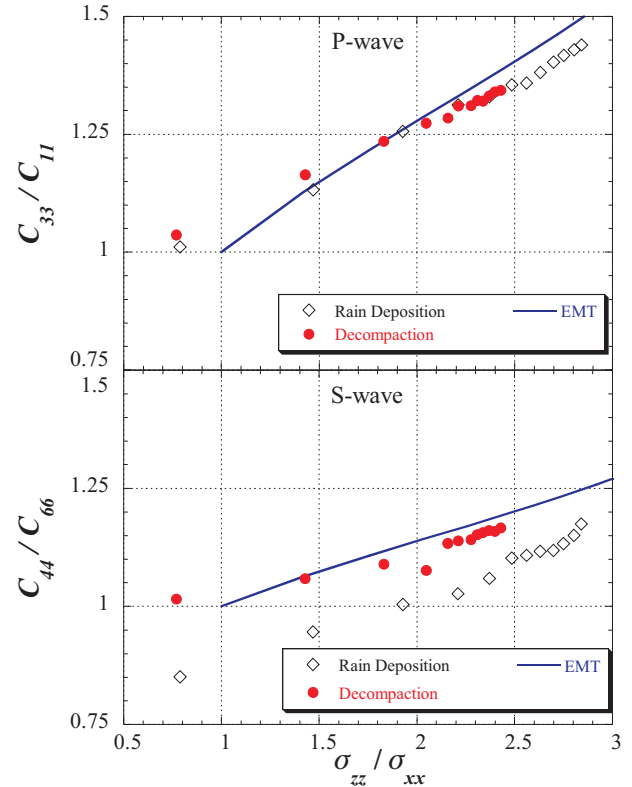


FIG. 8: Correlation between the induced elastic anisotropy and stress-field anisotropy in the granular packs of different fabric.

## V. CONCLUSION

In summary, we have studied the anisotropic elasticity of dry glass bead packs using ultrasonic measurements. Both the influences of the fabric anisotropy and the stress anisotropy are investigated thanks to the granular samples of different inherent fabric under uniaxial loading in an oedometric cell. The stress anisotropy is characterized from the horizontal and vertical force measurements, whereas the elastic moduli are determined from velocity measurements of P- and S-waves propagating along the vertical and horizontal directions, respectively. For the range of the applied stress in this work, our results show clearly that the compressional modulus anisotropy is more sensitive to the stress field anisotropy while the shear modulus anisotropy is more sensitive to the fabric anisotropy.

We have tested the applicability of the effective medium theory to sound propagation associated with the incremental deformation. The predictions by the analytical model based on the affine approximation agree well with the measurements

of sound velocity. Moreover, our velocity measurements of compressional waves confirm the scaling behaviour on stress,  $V_P \sim P^{1/6}$ , where  $P$  is the normal component of the stress along the propagation direction. As for the shear waves, the stress dependences of velocities are more complex, being also strongly influenced by the fabric anisotropy which is not considered in existing analytical EMT models.

The present effective medium model is also applied to analyze the finite deformation of the granular pack. Our stress-strain measurements show the breakdown of this model to describe adequately the deformed state at large deformation. However, such discrepancy between theory and experiment can significantly be reduced when the friction between grains is switched off. As indicated previously [4, 33], our observation confirms that the model based on the affine approximation fails because it prevents the relaxation of the tangential stress at the grain contact, especially for large deformation. Other effective medium models are required for describing the large deformations of granular packs [6, 12].

- 
- [1] J. D. Goddard, Proc. R. Soc. Lond. A **430**, 105 (1990).
  - [2] H. M. Jaeger, S. R. Nagel, and R. P. Behringer, Rev. Mod. Phys. **68**, 1259 (1996).
  - [3] P.-G. de Gennes, Rev. Mod. Phys. **71**, S374 (1999).
  - [4] H. A. Makse, N. Gland, D. L. Johnson, and L. Schwartz, Phys. Rev. E **70**, 061302 (2004).
  - [5] C. Goldenberg and I. Goldhirsch, Nature **435**, 188 (2005).
  - [6] Y. M. Jiang and M. Liu, Phys. Rev. Lett. **99**, 105501 (2007).
  - [7] A. N. Norris and D. L. Johnson, J. Appl. Mech. **64**, 39 (1997).
  - [8] X. Jia, C. Caroli, and B. Velický, Phys. Rev. Lett. **82**, 1863 (1999).
  - [9] E. Somfai, J.-N. Roux, J. H. Snoeijer, M. van Hecke, and W. van Saarloos, Phys. Rev. E **72**, 021301 (2005).
  - [10] E. Hoque and F. Tatsuoka, Soils and Foundations **38**, 163 (1998).
  - [11] R. García-Rojo, F. Alonso-Marroquín, and H. J. Herrmann, Phys. Rev. E **72**, 041302 (2005).
  - [12] P.-Y. Hicher and C. S. Chang, J. Geotech. Geoenviron. Eng. **132**, 1052 (2006).
  - [13] L. Vanel, D. Howell, D. Clark, R. P. Behringer, and E. Clément, Phys. Rev. E **60**, R5040 (1999).
  - [14] Y. Grasselli and H. J. Herrmann, Physica A **246**, 301 (1997).
  - [15] I. Ishibashi and O. F. Capar, Soils and Foundations **43**, 149 (2003).
  - [16] T. S. Majmudar and R. P. Behringer, Nature **435**, 1079 (2005); T. S. Majmudar, M. Sperl, S. Luding, and R. P. Behringer, Phys. Rev. Lett. **98**, 058001 (2007).
  - [17] F. Radjaï and S. Roux, in *Powders & Grains 2001*, edited by Y. Kishino (Balkema, Rotterdam, 2001), pp. 21–24.
  - [18] B. Cambou, Ph. Dubujet, and C. Noguier-Lehon, Mechanics of Materials **36**, 1185 (2004).
  - [19] S. Luding, Int. J. Sol. Struct. **41**, 5821 (2004).
  - [20] P.-E. Peyneau and J.-N. Roux, Phys. Rev. E **78**, 041307 (2008).
  - [21] M. N. Toksöz and D. H. Johnston, *Seismic Wave Attenuation* (Society of Exploration Geophysicists, Tulsa, OK, 1981).
  - [22] K. W. Winkler, Geophys. Res. Lett. **10**, 1073 (1983).
  - [23] R. A. Guyer and P. A. Johnson, Phys. Today **52**, 30 (1999); L. A. Ostrovsky and P. A. Johnson, Riv. Nuovo Cimento **24**, 1 (2001).
  - [24] L. E. Gilchrist, G. S. Baker, and S. Sen, Appl. Phys. Lett. **91**, 254103 (2007).
  - [25] C. H. Liu and S. R. Nagel, Phys. Rev. Lett. **68**, 2301 (1992); Phys. Rev. B **48**, 15646 (1993).
  - [26] X. Jia, Phys. Rev. Lett. **93**, 154303 (2004); Th. Brunet, X. Jia, and P. Mills, Phys. Rev. Lett. **101**, 138001 (2008).
  - [27] L. Bonneau, B. Andreotti, and E. Clément, Phys. Rev. E **75**, 016602 (2007).
  - [28] K. Walton, J. Mech. Phys. Solids **35**, 213 (1987).
  - [29] D. L. Johnson, L. M. Schwartz, D. Elata, J. G. Berryman, B. Hornby, and A. N. Norris, J. Appl. Mech. **65**, 380 (1998).
  - [30] J. Duffy and R. D. Mindin, J. Appl. Mech. **24**, 585 (1957).
  - [31] P. J. Digby, J. Appl. Mech. **48**, 803 (1981).
  - [32] S. N. Domenico, Geophysics **42**, 1339 (1977).
  - [33] J. Jenkins, D. Johnson, L. L. Ragione, and H. Makse, J. Mech. Phys. Solid **53**, 197 (2004).
  - [34] S. Emam, J.-N. Roux, J. Canou, A. Corfdir, and J.-C. Dupla, in *Powders & Grains 2005*, edited by R. Garcia-Rojo, H. Herrmann, and S. McNamara (Balkema, London, 2005), pp. 49–52.
  - [35] G. Reydellet, Ph.D. thesis, Université Paris 6 (2002); A. P. F. Atman, P. Brunet, J. Geng, G. Reydellet, G. Combe, P. Claudin, R. P. Behringer, and E. Clément, J. Phys.: Condens. Matter **17**, S2391 (2005).
  - [36] G. R. McDowell and A. Humphreys, Granular Matter **4**, 1 (2002).
  - [37] R. L. Michalowski, J. Geotech. Geoenviron. Eng. **131**, 1429 (2005).
  - [38] P. Evesque, D. Fargeix, P. Habib, M. Luong, and P. Porion, Phys. Rev. E **47**, 2326 (1993).
  - [39] X. Jia and P. Mills, in *Powders & Grains 2001*, edited by Y. Kishino (Balkema, Lisse, 2001), pp. 105–112.
  - [40] Th. Brunet, X. Jia, and P. A. Johnson, Geophys. Res. Lett. **35**, L19308 (2008).
  - [41] D. Royer and E. Dieulesaint, *Elastic Waves in Solids - Vol. 1: Free and Guided Propagation* (Springer, Berlin, 2000).



- [42] K. L. Johnson, *Contact Mechanics* (Cambridge Univ. Press, Cambridge, 1985).
- [43] F. E. Richart, J. R. Hall, and R. D. Woods, *Vibrations of Soils and Foundations* (Prentice-Hall, Englewood Cliffs, NJ, 1970).
- [44] B. Gilles and C. Coste, Phys. Rev. Lett. **90**, 174302 (2003).
- [45] P.-G. de Gennes, Europhys. Lett. **35**, 145 (1996).
- [46] B. Velický and C. Caroli, Phys. Rev. E **65**, 021307 (2002).